Zhang et al. Nanoscale Research Letters (2017) 12:393
DOI 10.1186/s11671-017-2164-z

Nanoscale Research Letters

NANO EXPRESS Open Access

Bipolar Resistive Switching Characteristics of $HfO_2/TiO_2/HfO_2$ Trilayer-Structure RRAM Devices on Pt and TiN-Coated Substrates Fabricated by Atomic Layer Deposition

Wei Zhang[1], Ji-Zhou Kong[1], Zheng-Yi Cao[1], Ai-Dong Li[1*], Lai-Guo Wang[1,2], Lin Zhu[1], Xin Li[1], Yan-Qiang Cao[1] and Di Wu[1]

Abstract

The $HfO_2/TiO_2/HfO_2$ trilayer-structure resistive random access memory (RRAM) devices have been fabricated on Pt- and TiN-coated Si substrates with Pt top electrodes by atomic layer deposition (ALD). The effect of the bottom electrodes of Pt and TiN on the resistive switching properties of trilayer-structure units has been investigated. Both $Pt/HfO_2/TiO_2/HfO_2/Pt$ and $Pt/HfO_2/TiO_2/HfO_2/TiN$ exhibit typical bipolar resistive switching behavior. The dominant conduction mechanisms in low and high resistance states (LRS and HRS) of both memory cells are Ohmic behavior and space-charge-limited current, respectively. It is found that the bottom electrodes of Pt and TiN have great influence on the electroforming polarity preference, ratio of high and low resistance, and dispersion of the operating voltages of trilayer-structure memory cells. Compared to using symmetric Pt top/bottom electrodes, the RRAM cells using asymmetric Pt top/TiN bottom electrodes show smaller negative forming voltage of −3.7 V, relatively narrow distribution of the set/reset voltages and lower ratio of high and low resistances of 10^2. The electrode-dependent electroforming polarity can be interpreted by considering electrodes' chemical activity with oxygen, the related reactions at anode, and the nonuniform distribution of oxygen vacancy concentration in trilayer-structure of $HfO_2/TiO_2/HfO_2$ on Pt- and TiN-coated Si. Moreover, for $Pt/HfO_2/TiO_2/HfO_2/TiN$ devices, the TiN electrode as oxygen reservoir plays an important role in reducing forming voltage and improving uniformity of resistive switching parameters.

Keywords: Atomic layer deposition, Resistive random access memory, Bottom electrode, Resistive switching parameters, Oxygen vacancy concentration, Trilayer structure

Background

Resistive random access memory (RRAM) has attracted great attention due to its potential for the replacement of flash memory in next-generation nonvolatile memories [1–3]. Resistive switching (RS) phenomenon has been widely discovered in transition metal oxides, solid electrolytes, and organic polymers [4–7]. RRAM devices based on transition metal oxides have been extensively explored because of its simple composition and compatible processing with conventional complementary metal-oxide-semiconductor (CMOS) fabrication [8–10]. The filament model of oxygen vacancy migration is used to elucidate the switching behavior [1, 11]. A unified microscopic principle is proposed to quantify both unipolar and bipolar switching characteristics of transition metal oxide-based RRAM, which are correlated with the distribution of localized oxygen vacancies in the oxide switching layer [12, 13].

However, memory cells using transition metal oxides suffer from nonuniformity of resistive switching parameters, such as unstable resistance values of low and high resistance states (LRS and HRS), dispersed set and reset

* Correspondence: adli@nju.edu.cn
[1]National Laboratory of Solid State Microstructures, Materials Science and Engineering Department, College of Engineering and Applied Sciences, Collaborative Innovation Center of Advanced Microstructures, Nanjing University, Nanjing 210093, People's Republic of China
Full list of author information is available at the end of the article

voltages, impeding the commercial applications. Recently, the trilayer-structure oxide-based RRAM devices have been demonstrated to improve the dispersion of resistive switching parameters. The cells with a structure of $Al_2O_3/HfO_2/Al_2O_3$ exhibited fantastic uniformity of set and reset voltages, and excellent endurance of switching between the LRS and HRS [14]. The linkage or rupture of the conductive filaments more easily occurred in two interfacial layers between Al_2O_3/IL/HfO_2/IL/Al_2O_3. Meanwhile, the unit of trilayer-structure of $TaO_x/TiO_2/TaO_x$ showed good performance in one selector-one resistor arrays, which was ascribed to the fact that the energy band of the TiO_2 film was symmetrically bent at the top and bottom TaO_x/TiO_2 interfaces and modified as a crested oxide barrier due to some Ta atoms diffusion into TiO_2 film [15].

Moreover, the RS behavior of a given oxide storage medium can be significantly affected by the electrode materials [1, 16, 17]. However, the existing models based on the free energy of interfacial oxide formation and the metal work functions are insufficient to completely explain the results. Meanwhile, the work on the electrodes dependent RS phenomenon of the trilayer-structure RRAM is also rather lacking at present.

Atomic layer deposition (ALD) is a new type of thin film deposition technology based on sequential self-limited and complementary surface chemisorptions reactions using precursor vapor with simple and precision thickness control, large area uniformity, and excellent three-dimensional conformality, especially for deposition of nano-laminated structure [18, 19].

In this work, the $HfO_2/TiO_2/HfO_2$ trilayer-structure RRAM devices have been prepared on Si/SiO_2/Ti/Pt and Si/TiN substrates with Pt top electrodes by ALD. The impact of the bottom electrodes of Pt and TiN on the RS behaviors of $HfO_2/TiO_2/HfO_2$ devices has been investigated carefully. The related explanation has been proposed.

Methods

In this experiment, we used two different bottom electrodes, including commercial Si/SiO_2/Ti/Pt and homemade Si/SiO_2/TiN. Conductive TiN was deposited by plasma-enhanced atomic layer deposition (PEALD) in our laboratory.

ALD was performed in a commercial Picosun SUNALE^{TM}R-200 advanced reactor (Picosun, Finland). *P* type Si (100) wafers with a resistivity of 1~10 Ω cm were used as the starting substrates. After the conventional RCA cleaning of the Si wafers without removing native oxide, 30-nm-thick TiN was deposited on Si as the bottom electrode at 400 °C by PEALD, using room temperature $TiCl_4$ and NH_3 plasma gas as the Ti and N precursors, respectively. Liquid NH_3 was selected as NH_3 plasma source at room temperature. The plasma power and NH_3 gas flow rate were 2500 W and 150 sccm, respectively.

Subsequently, 5 nm HfO_2/10 nm TiO_2/5 nm HfO_2 stacking structures were deposited in turn on Pt- and TiN-coated Si substrates at 250 °C by thermal ALD using $Hf[N(C_2H_5)CH_3]_4$ (TEMAH), $TiCl_4$, and H_2O as the Hf, Ti, and O precursors, respectively, where one oxide cycle consisted of 0.1*s* metal source injection, 4*s* N_2 purging, 0.1*s* H_2O injection, and 4*s* N_2 purging. TEMAH was evaporated at 150 °C. Pure N_2 (99.999%) was used as carrier gas and purging gas. Then, 100-nm-thick Pt top electrodes were DC sputtered through a shadow mask with a diameter of 150 μm using the Q150T system.

The growth per cycle (GPC) of pure HfO_2 or TiO_2 on Si was determined by spectroscopic ellipsometer (GES-5, Sopra). The topography and surface roughness of the films and bottom electrodes were analyzed by atomic force microscopy (AFM, Cypher, Asylum Research). The root-mean-square (RMS) roughness values were recorded from 1 μm × 1 μm areas. The composition and chemical state of the stack structures were examined by X-ray photoelectron spectroscopy (XPS, Thermo Fisher K-Alpha) with a monochromatic Al K_α source (hν = 1486.6 eV) for excitation of photoelectrons. The charge effect was calibrated by setting the C 1*s* photoemission at 284.6 eV. The XPS depth profile of $HfO_2/TiO_2/HfO_2$ on Pt- and TiN-coated Si was obtained by Ar ion etching. The electrical properties of the $HfO_2/TiO_2/HfO_2$ trilayer-structure RRAM devices were measured by Keithely 4200 semiconductor characterization system on probe station (CasCade Summit 12000 B-M). A current compliance of 10 mA was imposed to protect the fabricated device units from damages of high current during set processes. The bias voltage was applied to the Pt top electrode with the grounded bottom electrodes of Pt or TiN.

Results and Discussion

The schematic of the RRAM device of $HfO_2/TiO_2/HfO_2$ trilayer-structure by ALD is illustrated in Fig. 1. The

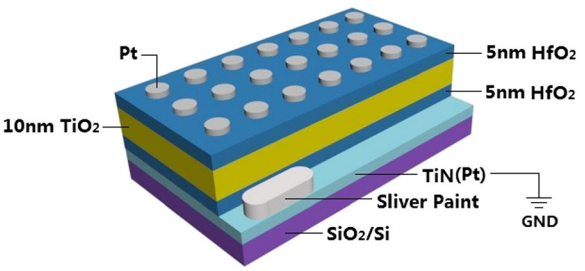

Fig. 1 The schematic of the RRAM device of $HfO_2/TiO_2/HfO_2$ trilayer-structure by ALD

surface morphology and roughness of the bottom electrodes and trilayer-structure of $HfO_2/TiO_2/HfO_2$ on Pt- and TiN-coated Si have been examined. The Pt bottom electrode has smaller RMS value of 0.39 nm than PEALD-derived TiN of 0.87 nm. Hence, the sample of $HfO_2/TiO_2/HfO_2$ on Pt-coated Si also exhibits relatively smoother surface with RMS of 0.68 nm than that on TiN-coated Si with 1.3 nm.

The DC I-V curves of $Pt/HfO_2/TiO_2/HfO_2/Pt$ and $Pt/HfO_2/TiO_2/HfO_2/TiN$ devices containing the initial electroforming process are plotted in Fig. 2a, b, respectively, indicating a typical bipolar resistive switching characteristic. For almost all the samples, larger forming voltage is needed to form conductive filaments before the switching test. When applying a positive bias voltage on the Pt top electrode, the $Pt/HfO_2/TiO_2/HfO_2/Pt$ device unit shows a forming voltage of +7 V in Fig. 2a. With continuing the voltage sweeping, a reset voltage of −0.8 V is measured for unit cell from LRS to HRS and a set voltage of 2.0 V from HRS to LRS. The corresponding ratio of high and low resistances is about 10^5. The electroforming and rest process can also be completed by applying a negative voltage of −11 V and a positive one of +4 V, respectively, which are much larger than the positive forming and negative reset voltages. Moreover, the device cell only switches from LRS to HRS for several cycles after the negative forming process and then fails to reset to HRS due to the irreversible breakdown (not shown here). In Fig. 2b, compared to that with symmetric Pt top and bottom electrodes, the trilayer structure RRAM devices with asymmetric TiN bottom electrode and Pt top electrode show an opposite lower forming voltage of about −3.7 V, set voltage of −1.5 V, reset voltage of +1.5 V, and relatively smaller ratio of high and low resistances of 10^2. When imposing the positive electroforming voltage, the RS phenomenon cannot be observed in the $Pt/HfO_2/TiO_2/HfO_2/TiN$ cell and the device is permanently broken down at +14 V without the following efficient reset from LRS to HRS at negative voltage (not shown here).

The trilayer-structure RRAM devices with symmetric Pt top/bottom electrodes and asymmetric TiN bottom electrode/Pt top electrodes exhibit such different electroforming polarity preference. The bottom electrode of chemically inert Pt or relatively active TiN seems to play a key role. The related reason on electrode-dependent electroforming polarity will be discussed later after considering the XPS depth profiles of trilayer structures of $HfO_2/TiO_2/HfO_2$ on Pt- and TiN-coated Si.

For high-density memory application, uniformity of RS parameters is very important. Figure 3a, b plots the statistical results of distribution of the set and reset voltages measured from a single device unit of the $Pt/HfO_2/TiO_2/HfO_2/Pt$ and $Pt/HfO_2/TiO_2/HfO_2/TiN$ for 200 times tests, respectively. Figure 3c, d records the I–V curves of 10 randomly selected device units of the $Pt/HfO_2/TiO_2/HfO_2/Pt$ and $Pt/HfO_2/TiO_2/HfO_2/TiN$, respectively. The trilayer-structure RRAM device units with symmetric Pt top and bottom electrodes show a broad distribution for set voltage from 1.2 to 2.8 V and reset voltage from −0.5 to −1 V (Fig. 3a) and dispersive I–V curves (Fig. 3c). Whereas, the device units with asymmetric TiN bottom and Pt top electrodes display better RS behavior, such as relatively concentrated distribution of set voltage from −0.8 to −1.8 V and reset voltage from 1.3 to 1.8 V, and stable reproducibility in I–V curves (Fig. 3b, d). Simultaneously, compared to those on Pt-coated Si, different device units on TiN-coated Si also behave improved monodispersion in RS parameters, beneficial to RRAM practical applications.

The endurance and retention properties of the device units of $Pt/HfO_2/TiO_2/HfO_2/Pt$ and $Pt/HfO_2/TiO_2/HfO_2/TiN$ have been examined, as seen in Fig. 4a–d, respectively. In $Pt/HfO_2/TiO_2/HfO_2/Pt$, the sweeping voltage was applied from 0 to 3 V for set and 0 to −1.5 V for reset. In $Pt/HfO_2/TiO_2/HfO_2/TiN$, the sweeping voltage was applied from 0 to −2 V for set and 0 to 2 V for reset. The ON and OFF resistance values were read using 0.2 V at room temperature. The retention tests were measured at room temperature with the reading voltage

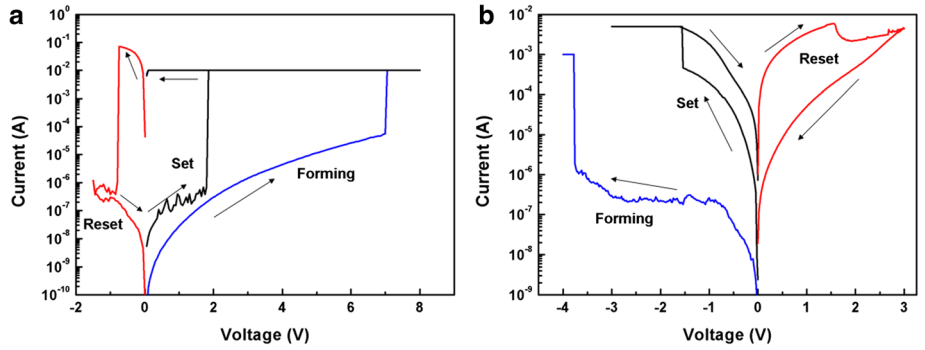

Fig. 2 The typical bipolar resistive switching characteristics of the RRAM devices. **a** $Pt/HfO_2/TiO_2/HfO_2/Pt$. **b** $Pt/HfO_2/TiO_2/HfO_2/TiN$

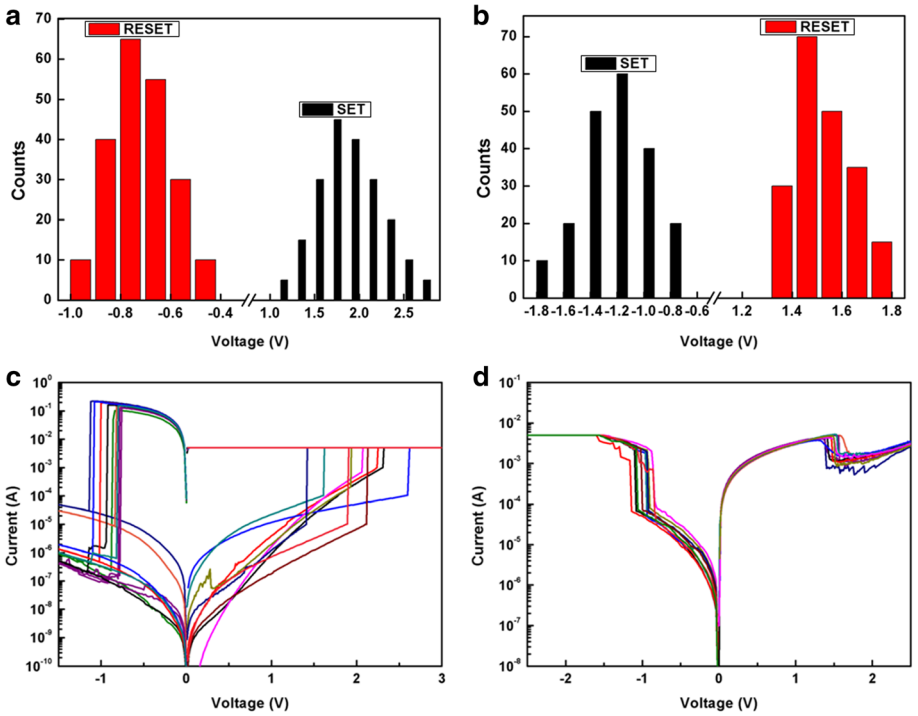

Fig. 3 The statistical results of distribution of the set and reset voltages measured from a single device unit for 200 times tests. **a** Pt/HfO_2/TiO_2/HfO_2/Pt. **b** Pt/HfO_2/TiO_2/HfO_2/TiN. The I–V curves of 10 randomly selected device units. **c** Pt/HfO_2/TiO_2/HfO_2/Pt. **d** Pt/HfO_2/TiO_2/HfO_2/TiN

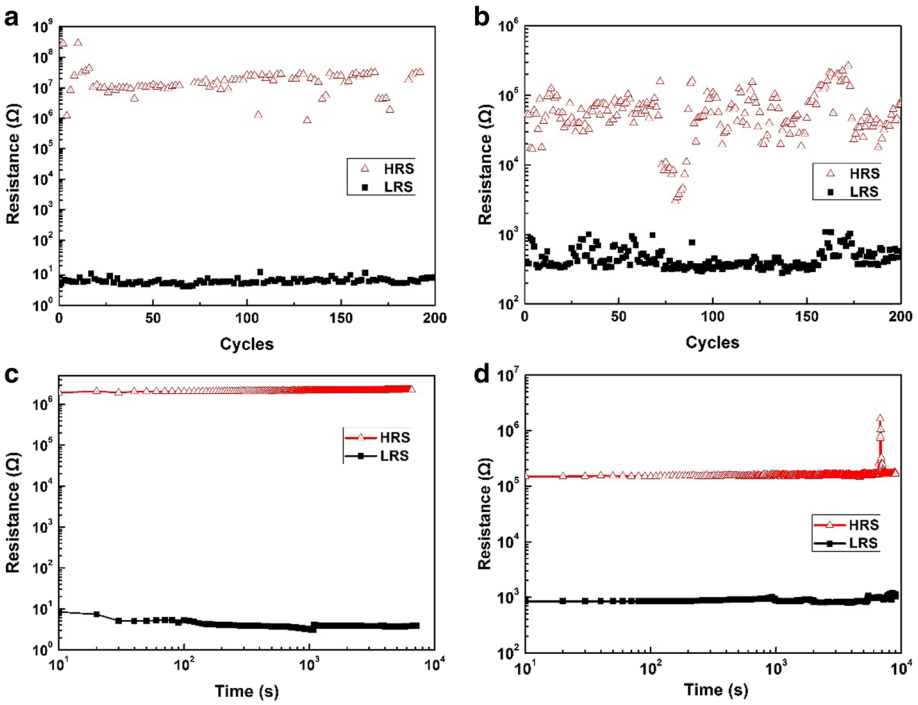

Fig. 4 The endurance and retention characteristics of the device units. **a**, **c** Pt/HfO_2/TiO_2/HfO_2/Pt. **b**, **d** Pt/HfO_2/TiO_2/HfO_2/TiN.

of 0.2 V. After 200 program/erase cycles, $Pt/HfO_2/TiO_2/HfO_2/Pt$ device units show relatively stable resistance ratio of OFF/ON states above 10^5 (Fig. 4a); however, the endurance characteristic of $Pt/HfO_2/TiO_2/HfO_2/TiN$ memory cells seem not to be as good as that of $Pt/HfO_2/TiO_2/HfO_2/Pt$ (Fig. 4b). The ON and OFF states in devices with Pt-TiN electrodes are not very steady with smaller resistance ratio of OFF/ON states of about 10^2 during switching cycle test, especially significant HRS fluctuation than that of LRS. Based on the physical model in Ref. [12], the endurance will be improved by increasing the formation energy of oxygen vacancy and interface O^{2-} amount. We speculate one plausible explanation. In our previous work [14], excellent bipolar resistive switching properties of ALD-derived $Al_2O_3/HfO_2/Al_2O_3$ trilayer-structures with asymmetric TiN bottom and Pt top electrodes have been demonstrated, including better switching endurance up to 10^3 cycles with stable ON/OFF resistance ratio. Herein, we adopted $HfO_2/TiO_2/HfO_2$ configure instead of $Al_2O_3/HfO_2/Al_2O_3$. The metal ions in HfO_2 and TiO_2 have the same identical chemical valence of +4, leading to the less interface charged defects such as oxygen vacancies between two interfacial layers (ILs) of trilayer $HfO_2/TiO_2/HfO_2$. Whereas, the metal ions in Al_2O_3 and HfO_2 have different chemical valence of Al^{3+} and Hf^{4+}, producing more interface charged defects of oxygen vacancies between two ILs of $Al_2O_3/HfO_2/Al_2O_3$. It can be deduced that the interface O^{2-} amount by adding two ILs between $Al_2O_3/HfO_2/Al_2O_3$ should be higher than between $HfO_2/TiO_2/HfO_2$. In addition, the formation energy of oxygen vacancy in storage layer of $Al_2O_3/HfO_2/Al_2O_3$ is also higher than that of $HfO_2/TiO_2/HfO_2$ (formation energy of oxygen vacancy 7.08 eV (Al_2O_3), 6.53 eV (HfO_2), and 4.35 eV (TiO_2) [20, 21]). After considering these factors, the memory cell of $Pt/HfO_2/TiO_2/HfO_2/TiN$ exhibits endurance degeneration, compared to $Pt/Al_2O_3/HfO_2/Al_2O_3/TiN$.

For $Pt/HfO_2/TiO_2/HfO_2/Pt$ and $Pt/HfO_2/TiO_2/HfO_2/TiN$, the resistance level of the ON and OFF states has no evident changes after cumulative waiting time of 10^4 s at room temperature in Fig. 4c–d, indicating a better retention property of both memory cells over 10 years based on the extrapolation method.

$Pt/HfO_2/TiO_2/HfO_2/TiN$ devices have much lower resistance ratio of OFF/ON states than $Pt/HfO_2/TiO_2/HfO_2/Pt$, which can be attributed to the difference of the bottom electrodes in work function and conductivity. The work function of Pt and TiN bottom electrodes is 5.65 and 4.5 eV, respectively; hence, the interface barrier between TiN and underlying HfO_2 is relatively lower in the $Pt/HfO_2/TiO_2/HfO_2/TiN$ device. During a reset process, the needed energy for electron to cross the barrier is also smaller. So $Pt/HfO_2/TiO_2/HfO_2/TiN$ manifests lower resistance value in OFF state than $Pt/HfO_2/TiO_2/HfO_2/Pt$ correspondingly. During a set process, RRAM device changes from HRS into LRS owing to the formation of the conducting channels. The Pt bottom electrode has higher conductivity than TiN bottom one; accordingly, the resistance value in ON state for $Pt/HfO_2/TiO_2/HfO_2/TiN$ is higher than that for $Pt/HfO_2/TiO_2/HfO_2/Pt$. As a result, $Pt/HfO_2/TiO_2/HfO_2/TiN$ devices show a smaller resistance ratio of OFF/ON states of 10^2. However, the resistance ratio of 10^2 has already met the requirement of RRAM applications.

To clarify the conductive mechanism during resistive switching, the typical I–V curves are replotted in double-logarithmic scale. Figure 5a, b shows the linear fitting of the I–V curves for the voltage sweeping regions of $Pt/HfO_2/TiO_2/HfO_2/Pt$ and $Pt/HfO_2/TiO_2/HfO_2/TiN$ devices. Both memory cells behave similar conductive mechanism. When the device is switched to the LRS, the curves of log (I)-log (V) are linear with slope close to 1 (0.94 in Fig. 5a, 0.98 in Fig. 5b), indicating that the I–V at the LRS is dominated by the Ohmic law. The filament model of oxygen vacancy migration can be used to explain the switching behavior. For the HRS, at low-voltage region (absolute value <0.11 V), the I–V is dominated by the Ohmic law with the linear relationship of current and voltage (slope 1.05 in Fig. 5a, 1.09 in Fig. 5b). At higher voltage region (6.8 V > absolute value >0.11 V in Fig. 5a, 1.85 V > absolute value >0.11 V in Fig. 5b), the slope of the log (I)-log (V) lines are around 2 and the current is dependent of approximate square of applied voltage (I/V^2). At critical voltage (absolute value 6.8 V in Fig. 5a, 1.85 V in Fig. 5b), a steep current rise suddenly appears with a very large slope. This result consists of three regions in HRS, basically obeying the typical trap-controlled space-charge-limited conduction (SCLC) injection [11].

In order to further understand the underlying resistive switching mechanism of $HfO_2/TiO_2/HfO_2$ on Pt-coated and TiN-coated Si, we performed the XPS narrow scans and depth analyses on trilayer structures with symmetric and asymmetric bottom/top electrodes. XPS spectra were fitted with Gaussian-Lorentzian (G-L) functions after smart-type background subtraction.

Figure 6a–d illustrates the narrow-scan XPS spectra of Hf 4*f*, Ti 2*p*, and O 1*s* peaks in HfO_2 and TiO_2 layers on TiN-coated Si. The Hf 4*f* and Ti 2p spectra from HfO_2 and TiO_2 layers can be deconvoluted into two group peaks. The stronger Hf $4f_{5/2}$ and Hf $4f_{7/2}$ peaks at 18.4 and 16.7 eV with a spin–orbit splitting of 1.7 eV are assigned to Hf–O bonding (Hf^{4+}) from HfO_2 (Fig. 6a). The weaker spin–orbit doublet peaks at lower binding energy of 17.6 and 14.8 eV possibly result from the low-chemical valence state of Hf^{n+}–O ($n < 4$), indicating the

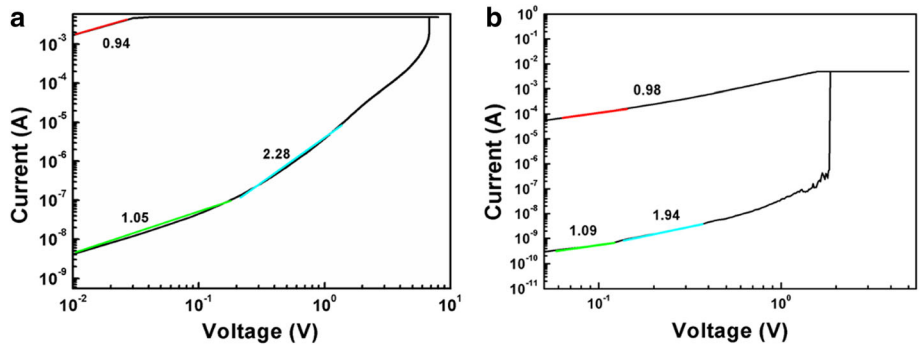

Fig. 5 The typical I–V curves plotted in double-logarithmic scale of **a** Pt/HfO_2/TiO_2/HfO_2/Pt and **b** Pt/HfO_2/TiO_2/HfO_2/TiN

presence of oxygen vacancies in HfO_2 layer. The calculated percentage concentration of Hf^{n+} ($n < 4$) is about 3.7% in Hf ions. In Fig. 6b, a stronger doublet corresponds to Ti 2*p*3/2 and 2*p*1/2 features at 458.8 and 464.5 eV, belonging to the Ti–O bonding (Ti^{4+}) from TiO_2. A weaker doublet locates at 456.1 and 462.0 eV, assigning to the Ti^{3+}–O bonding. The calculated percentage concentration of Ti^{3+} is about 21% in Ti ions. This implies the existence of oxygen vacancies in TiO_2 layer.

The O 1*s* spectra from HfO_2 and TiO_2 layers can also be deconvoluted into two peaks, as seen in Fig. 6c, d. The relatively lower binding energies of the O 1*s* peak at ~530.9 and 531.2 eV are assigned to Ti-O and Hf-O bonding in TiO_2 and HfO_2 layers, respectively, belonging to lattice oxygen without oxygen vacancies. Whereas the slightly higher energy of 532.1 eV in the O 1*s* spectra of Fig. 6c, d are ascribed to the oxygen atoms near oxygen vacancies in HfO_2 and TiO_2 layers based on the literature reports [22–25]. The relative oxygen vacancy concentration in the oxide layer can be roughly evaluated by calculating the area proportion of each peak [22, 23]. The calculated percentage concentration of oxygen vacancy in HfO_2 and TiO_2 layers is about 2.3 and 19.4%, respectively, in accord with the results of Hf^{n+} and Ti^{3+}.

Figure 7a, b shows the XPS depth profiles of HfO_2/TiO_2/HfO_2 samples on Pt- and TiN-coated Si by Ar ion

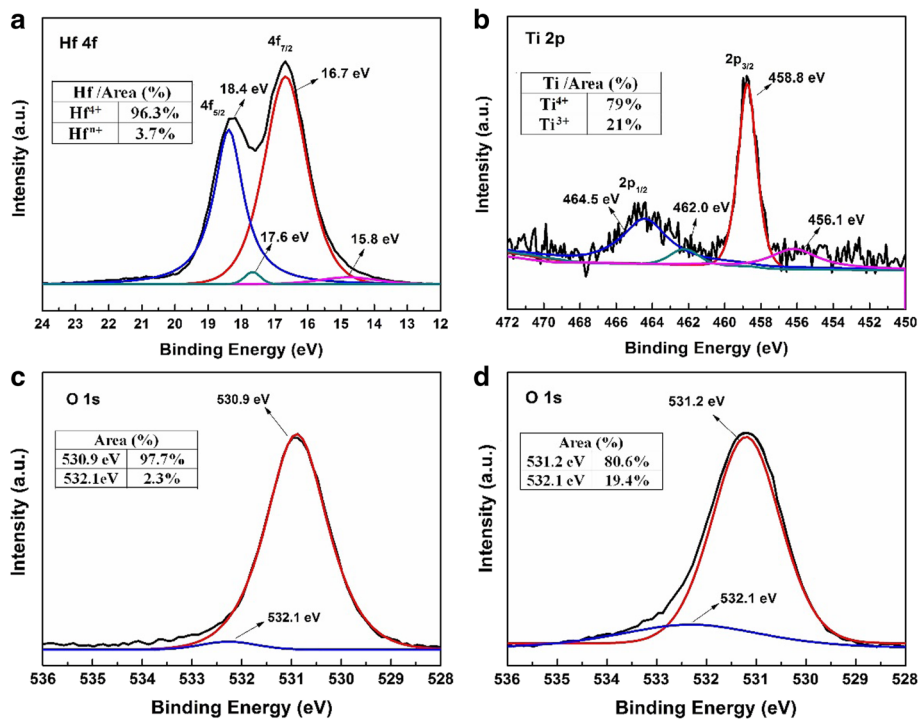

Fig. 6 Narrow-scan XPS spectra from trilayer-structure of HfO_2/TiO_2/HfO_2 on TiN-coated Si. **a** Hf 4f, **b** Ti 2*p* peaks of HfO_2/TiO_2/HfO_2. O 1*s* peaks of **c** HfO_2 and **d** TiO_2 layers

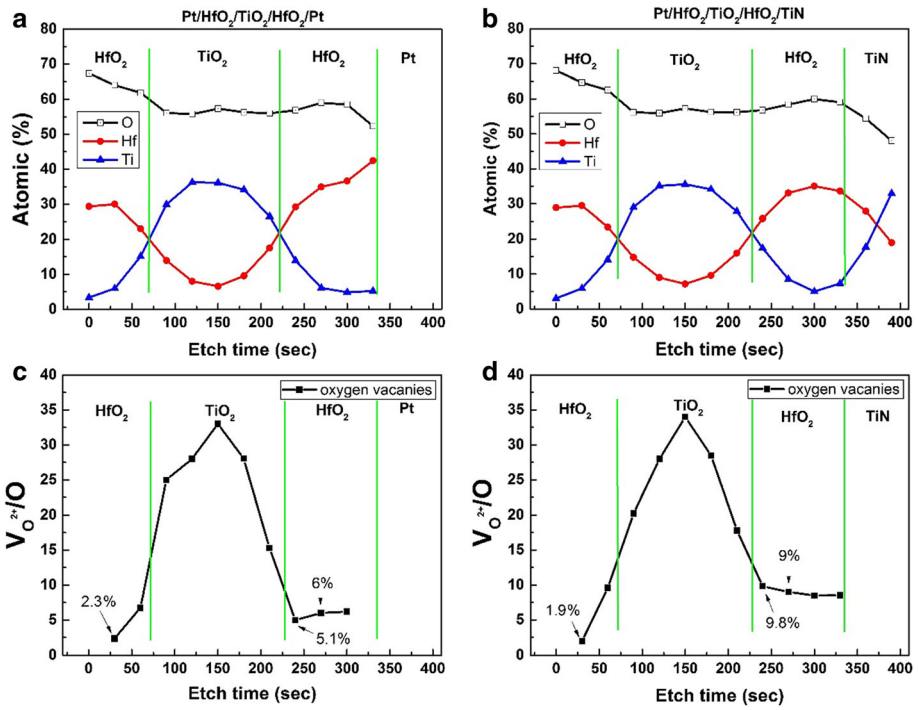

Fig. 7 XPS depth profiles of $HfO_2/TiO_2/HfO_2$ on Pt- and TiN-coated Si by Ar ion etching. **a** $HfO_2/TiO_2/HfO_2$ on Pt-coated Si. **b** $HfO_2/TiO_2/HfO_2$ on TiN-coated Si. The depth distribution of oxygen vacancy concentration (V_O^{2+}/O) determined from XPS spectra for $HfO_2/TiO_2/HfO_2$ on Pt- and TiN-coated Si. **c** $HfO_2/TiO_2/HfO_2$ on Pt-coated Si. **d** $HfO_2/TiO_2/HfO_2$ on TiN-coated Si

etching, respectively. The trilayer-structure of $HfO_2/TiO_2/HfO_2$ on Pt- and TiN-coated Si can be recognized easily, although the significant interfacial diffusion between HfO_2/TiO_2 and HfO_2/TiN has been observed. Usually the filament model of oxygen vacancy migration dominates the RS behavior in RRAM devices based on transition metal oxides [11]. However, simply increasing the oxygen vacancies content is not fully effective. How to effectively control the distribution of oxygen vacancy filaments is a key issue to finally improving the RS uniformity [20]. Lots of work has shown that usually a nonuniform distribution of oxygen vacancies is beneficial to the RS behaviors, including decreasing the forming voltage, improving the switching stability and endurance ability [1, 14, 20, 26–29]. An initial nonuniform distribution of oxygen vacancies in a storage oxide layer is often obtained by the use of a chemically active electrode with a relatively high oxygen affinity (e.g., Ta, Ti, Al, or TiN) or by deliberately introducing an oxygen vacancy-rich interfacial layer by interface engineering [1, 17, 30].

Figure 7c, d presents the distribution curves of oxygen vacancy concentration of $HfO_2/TiO_2/HfO_2$ on Pt- and TiN-coated Si based on the above depth XPS profiles, respectively. The oxygen vacancy concentration was evaluated using the method mentioned above. It can be found that the highest oxygen vacancy concentration (~34%) appears in TiO_2 intermediate layer. Another noteworthy feature is that the underlying HfO_2 layer near Pt or TiN bottom electrodes has higher oxygen vacancy concentration than upper HfO_2 layer (~2%). Besides, the oxygen vacancy concentration (~9%) of underlying HfO_2 layer on TiN-coated Si is obviously higher than that (~6%) on Pt-coated Si.

Figure 8 shows the schematic diagrams of electroforming and reset of $Pt/HfO_2/TiO_2/HfO_2/Pt$ at positive and negative bias voltages. For chemically inert Pt top and bottom electrodes, the bias polarity-dependent electroforming phenomena are related to the O_2 gas released from the oxide layer at the anode as a product of electroreduction. As known, during electroforming process, oxygen vacancies are created by high electric field and migrate to the cathode, forming localized conducting filaments in the oxide layer, i.e., $O_O \rightarrow V_O^{2+} + O^{2-}$, $V_O^{2+} + 2e^- \rightarrow V_O$ [12] (Fig. 8b, e). Simultaneously, O^{2-} ions drift towards the anode, releasing their charge and evolving O_2 gas, i.e., $O^{2-} \rightarrow 1/2O_2 + 2e^-$ (Fig. 8b, e), which possibly cause physical deformation of the cell and even formation of crack or hole [31]. When applying positive forming voltage to Pt top electrode, we postulate the O_2 gas released above the upper HfO_2 film easily escapes at the top electrode edge or through small nanopore in Pt top electrode (Fig. 8b), which causes weak physical deformation.

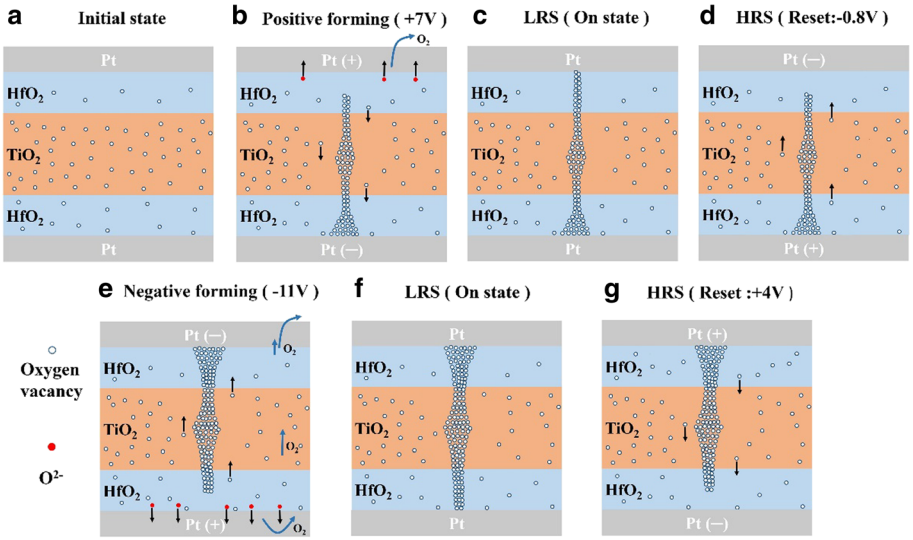

Fig. 8 Schematic diagrams of electroforming and reset of trilayer-structure of $HfO_2/TiO_2/HfO_2$ with symmetric Pt top and bottom electrodes. **a**–**d** Electroforming at positive voltage and reset at negative voltage. **e**–**g** Electroforming at negative voltage and reset at positive voltage

Meanwhile, considering the relatively higher oxygen vacancy concentration in underlying HfO_2 (~6%) nearby Pt bottom electrode than the upper HfO_2 layer (~2.3%) (Fig. 7c), the conductive filament readily forms, leading to smaller positive forming voltage of +7 V. With reverse voltage of −0.8 V, the reverse reaction leads to the filament ruptures, and the device is easily switched back to the HRS state (Fig. 8d).

Conversely, with a negative forming voltage on the top electrode, oxygen gas forms under the underlying HfO_2 layer and above Pt the bottom electrode (Fig. 8e). The O_2 releasing becomes more difficult, which will impede the formation of conductive filaments. Moreover, because the oxygen vacancy concentration of the upper HfO_2 layer (~2.3%) is lower than that of the underlying HfO_2 (~6%) (Fig. 7c), the higher negative forming voltage of −11 V is needed to form filaments. When more O_2 accumulates to a certain pressure under underlying HfO_2, it possibly erupts from the mechanically weakest part of the thin films, leading to the hole in oxide films or separation between oxide films and the bottom electrode induced by bubble cracking. Although the device can be reset to HRS at applied +4 V bias (Fig. 8g), the memory cell is degraded after several switching cycles. In our samples, a part of top electrode was blown off after the forming process. Similar electroforming polarity preference scenario has also been observed in $Pt/TiO_{2-x}/Pt$ bipolar RRAM cells with various physical deformation evidences of the junctions [31, 32].

$Pt/HfO_2/TiO_2/HfO_2/TiN$ devices exhibit quite different electroforming polarity from $Pt/HfO_2/TiO_2/HfO_2/Pt$. The LRS caused by electroforming can be observed at both negative and positive bias voltage; however, the effective reset from LRS to HRS can be achieved only at positive bias voltage in $Pt/HfO_2/TiO_2/HfO_2/TiN$ device. Similar electroforming preference with asymmetric Pt and TiN electrodes has been observed in some literatures with various storage oxide layers such as HfO_2 [33, 34], TiO_2 [35], ZrO_x/HfO_y bilayer [22], and $Al_2O_3/HfO_2/Al_2O_3$ trilayer [14]. However, the related explanations are divergent or lacking.

After considering the TiN electrode's chemical activity with oxygen [1, 30, 36] and the nondistribution of oxygen vacancy concentration in trilayer-structure of $HfO_2/TiO_2/HfO_2$ based on the XPS depth profiles (Fig. 7), a possible mechanism on electroforming polarity preference of $Pt/HfO_2/TiO_2/HfO_2/TiN$ cells is proposed. Figure 9 shows the schematic diagrams of electroforming and reset of $Pt/HfO_2/TiO_2/HfO_2/TiN$ at negative and positive bias voltages. The TiN bottom electrode plays a key role in the electroforming polarity. Kwak et al. reported that the relatively active TiN electrode would easily absorb oxygen ions from oxide films to form TiO_xN_{1-x} (TiON) interfacial layer [36]. The severe oxygen diffusion of underlying HfO_2 layer into TiN bottom electrode has been confirmed in our sample by the XPS depth profile (Fig. 7b). For $Pt/HfO_2/TiO_2/HfO_2/TiN$ device, the TiN electrode with high oxygen affinity [34, 36] produces a lot of oxygen vacancies in the underlying HfO_2 layer near the TiN bottom electrode. The oxygen vacancies concentration of ~9% of underlying HfO_2 layer is much higher than that of ~6% in the $Pt/HfO_2/TiO_2/HfO_2/Pt$ device.

For chemically inert Pt top electrode and relatively active TiN bottom electrode, when applying negative forming voltage, O^{2-} ions drift towards the TiN anode and

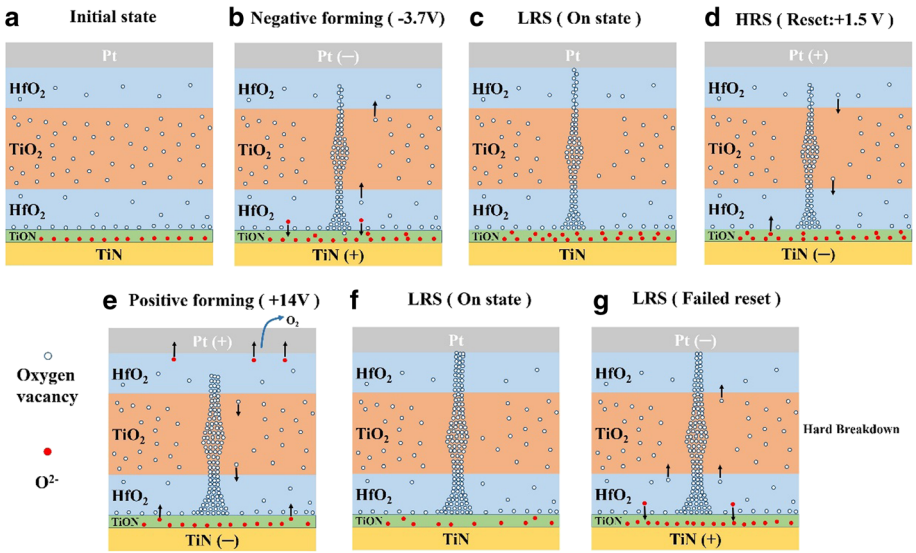

Fig. 9 Schematic diagrams of electroforming and reset of trilayer-structure of $HfO_2/TiO_2/HfO_2$ with asymmetric Pt top electrode and TiN bottom electrode. **a**–**d** Electroforming at negative voltage and reset at positive voltage. **e**–**g** Electroforming at positive voltage and reset at negative voltage

are absorbed to form TiO_xN_{1-x} layer (Fig. 9b), i.e., $TiN + xO^{2-} \rightarrow TiO_xN_{1-x} + x2e$, avoiding the O_2 release and possible damage to cells. The TiN electrode might act as a reservoir for oxygen ions drifting under an applied voltage [1, 36]. Simultaneously, due to the higher oxygen vacancy in the underlying HfO_2 layer (~9%) and intermediate TiO_2 layer (~10–34%) than the upper HfO_2 layer (~1.9%), the migration of the rich oxygen vacancies from the underlying HfO_2 layer through TiO_2 layer towards the the upper HfO_2 layer, directly producing conductive oxygen vacancy filaments with a smaller forming voltage of −3.7 V (Fig. 9b). When performing reverse reset process at +1.5 V, the bottom electrode of TiN layer acting as oxygen reservoir supplies oxygen ions to react with oxygen vacancy, i.e., $O^{2-} + V_O^{2+} \rightarrow O_O$ (lattice oxygen), which is beneficial to the reset operation from LRS to HRS with rupture of conductive filament (Fig. 9d). Above all, the oxygen reservoir effect of TiN bottom electrode contributes the forming voltage reduction as well as better set/reset voltage variation [1, 29, 36].

On the other hand, when imposing the positive forming voltage on top electrode Pt, the oxygen vacancies migrate from the upper HfO_2 into the underlying HfO_2 on TiN, accumulate in its vicinity, and develop into filaments. Owing to the lower oxygen concentration in the upper HfO_2 (~1.9%) than the underlying HfO_2 layer (~9%) and intermediate TiO_2 layer (~10–34%), this leads to further increase of the oxygen vacancy concentration in underlying HfO_2 and intermediate TiO_2 layer. In the same time, due to slight oxygen existence in PEALD-derived TiN films (about 10%), some oxygen ions in TiN drift into underlying HfO_2 layer to form insulate lattice oxygen with nearby oxygen vacancy, preventing from the growth of conductive filaments (Fig. 9e). Finally, when the bias voltage attains +14 V, the coarsening conductive filaments in oxides is formed. However, when a negative voltage is applied on the device, the conductive filament in trilayer structure is too large to be ruptured (Fig. 9g). Therefore, the device cannot switch to HRS by applying a negative voltage, indicating that an irreversible hard breakdown occurs in $Pt/HfO_2/TiO_2/HfO_2/TiN$ device.

Finally, on account of the fact that the inserted TiO_2 layer stores more oxygen vacancies than HfO_2 layer, the distribution of oxygen vacancies in trilayer structure is not uniform, especially in the two interfacial layers between $HfO_2/IL/TiO_2/IL/HfO_2$, which might affect the growth position, direction, and overlapping of conductive filaments. The linkage or rupture of the conductive filaments corresponds to the set process from HRS to LRS or the reset process from LRS to HRS, respectively, which more easily happens in two interfacial layers. Further, the shape and position of the conductive filaments in HfO_2 and TiO_2 layers change less in the set and reset processes.

Conclusions

In summary, RRAM devices based on trilayer-structure of $Pt/HfO_2/TiO_2/HfO_2/Pt$ and $Pt/HfO_2/TiO_2/HfO_2/TiN$ have been prepared by ALD. Both memory cells show typical bipolar resistive switching characteristics, and Ohmic and SCLC dominant conduction mechanisms in LRS and HRS, respectively. It is found that the bottom electrodes of Pt and TiN have great influence on the

electroforming polarity preference, the ratio of high and low resistances and dispersion of the operating voltage of trilayer-structure memory cells. Compared to with symmetric Pt top/bottom electrodes, the RRAM cells with asymmetric Pt top/TiN bottom electrodes show smaller negative forming voltage of −3.7 V, relatively narrow distribution of the set/reset operation voltages and lower ratio of high and low resistances of 10^2. The electrode-dependent electroforming polarity can be explained by considering electrodes' chemical activity with oxygen, the related reactions at anode, and the nonuniform distribution of oxygen vacancy concentration in trilayer-structure of $HfO_2/TiO_2/HfO_2$ on Pt- and TiN-coated Si. Furthermore, the TiN electrode as oxygen reservoir plays an important role in forming voltage reduction and better dispersion of RS parameters for Pt/$HfO_2/TiO_2/HfO_2$/TiN devices. Considering the modulation effect of electrode and trilayer-structure on resistive switching performance, this work provides a new device design route for future RRAM applications.

Acknowledgements
This project is supported by the Natural Science Foundation of China and Jiangsu Province (51571111 and BK2016230), a grant from the State Key Program for Basic Research of China (2015CB921203). Ai-Dong Li also thanks the support of Priority Academic Program Development in the Jiangsu Province.

Authors' Contributions
WZ, JZK, and ZYC carried out the sample fabrication and device measurements and drafted the manuscript. WZ, JZK, and ZYC analyzed the data and explained the results. WZ, JZK, and ZYC contributed equally to this work. LZ and XL helped to finish the X-ray photoelectron spectroscopy measurements. ADL, DW, and YQC participated in the discussion of results. ADL modified the manuscript and supervised all the projects. All authors read and approved the final manuscript.

Competing Interests
The authors declare that they have no competing interests.

Publisher's Note

Author details
[1]National Laboratory of Solid State Microstructures, Materials Science and Engineering Department, College of Engineering and Applied Sciences, Collaborative Innovation Center of Advanced Microstructures, Nanjing University, Nanjing 210093, People's Republic of China. [2]Anhui Key Laboratory of Functional Coordination Compounds, School of Chemistry and Chemical Engineering, Anqing Normal University, Anhui 246011, People's Republic of China.

Received: 31 December 2016 Accepted: 24 May 2017
Published online: 08 June 2017

References
1. Pan F, Gao S, Chen C, Song C, Zeng F (2014) Recent progress in resistive random access memories: materials, switching mechanisms, and performance. Mater Sci Eng R 83:1–59
2. Chang WY, Cheng KJ, Tsai JM, Chen HJ, Chen F, Tsai MJ, Wu TB (2009) Improvement of resistive switching characteristics in TiO_2 thin films with embedded Pt nanocrystals. Appl Phys Lett 95:042104
3. Waser R, Aono M (2007) Nanoionics-based resistive switching memories. Nat Mater 6:833–40
4. Song S, Cho B, Kim TW, Ji Y, Jo M, Wang G, Choe M, Kahng YH, Hwang H, Lee T (2010) Three dimensional integration of organic resistive memory devices. Adv Mater 22:5048–52
5. Jung R, Lee MJ, Seo S, Kim DC, Park GS, Kim K, Ahn S, Park Y, Yoo IK, Kim JS, Park BH (2007) Decrease in switching voltage fluctuation of Pt/NiO. Appl Phys Lett 91:022112
6. Chiu FC, Li PW, Chang WY (2012) Reliability characteristics and conduction mechanisms in resistive switching memory devices using ZnO thin films. Nanoscale Res Lett 7:178
7. Gao B, Kang J, Liu L, Liu X, Yu B (2011) A physical model for bipolar oxide-based resistive switching memory based on ion-transport-recombination effect. Appl Phys Lett 98:232108
8. Kim DK, Suh DS, Park J (2010) Pulse-programming instabilities of unipolar-type NiO_x. IEEE Electron Dev Lett 31:600–2
9. Miranda EA, Walczyk C, Wenger C, Schroeder T (2010) Model for the resistive switching effect in MIM structures based on the transmission properties of narrow constrictions. IEEE Electron Dev Lett 31:609–11
10. Shen W, Dittmann R, Breuer U, Waser R (2008) Improved endurance behavior of resistive switching in (Ba, Sr)TiO_3 thin films with W top electrode. Appl Phys Lett 93:222102
11. Yang JJ, Strukov DB, Stewart DR (2013) Memristive devices for computing. Nat Nanotech 8:13–24
12. Gao B, Kang JF, Chen Y S, Zhang FF, Chen B, Huang P, Liu LF, Liu XY, Wang YY, Tran XA, Wang ZR, Yu HY, and Chin A. Oxide-based RRAM: unified microscopic principle for both unipolar and bipolar switching. IEDM Tech Dig. 2011;11:417–20.
13. Gao B, Sun B, Zhang HW, Liu LF, Liu XY, Han RQ, Kang JF, Yu B (2009) Unified physical model of bipolar oxide-based resistive switching memory. IEEE Electron Dev Lett 30:1326–28
14. Wang LG, Qian X, Cao YQ, Cao ZY, Fang GY, Li AD, Wu D (2015) Excellent resistive switching properties of atomic layer-deposited $Al_2O_3/HfO_2/Al_2O_3$ trilayer structures for non-volatile memory applications. Nanoscale Res Lett 10:135
15. Lee WT, Park JB, Kim SH, Woo JY, Shin JH, Choi G, Park SS, Lee D, Cha E, Lee BH, Hwang HS (2012) High current density and nonlinearity combination of selection device based on $TaO_x/TiO_2/TaO_x$ structure for one selector-one resistor arrays. ACS Nano 6:8166–72
16. Uenuma M, Zheng B, Kawano K, Horita M, Ishikawa Y, Yamashita I, Uraoka Y (2012) Guided filament formation in NiO-resistive random access memory by embedding god nanoparticles. Appl Phys Lett 100:083105
17. Lin KL, Hou TH, Shieh J, Lin JH, Chou CT, Lee YJ (2011) Electrode dependence of filament formation in HfO_2 resistive-switching memory. J Appl Phys 109:084104
18. Puurunen RL (2005) Surface chemistry of atomic layer deposition: a case study for the trimethylaluminum/water process. J Appl Phys 97:121301
19. Sherman A (2008) Atomic layer deposition for nanotechnology: an enabling process for nanotechnology fabrication. Ivoryton Press, New York
20. Lian WT, Long SB, Lü HB, Liu Q, Li YT, Zhang S, Wang Y, Huo ZL, Dai YH, Chen JN, Liu M (2011) Approaches for improving the performance of filament-type resistive switching memory. Chin Sci Bull 56:461–464
21. Tanaka I, Oba F, Tatsumi K, Kunisu M, Nakano M, Adachi H (2002) Theoretical formation energy of oxygen-vacancies in oxides. Mater Trans 43:1426–29
22. Huang CY, Huang CY, Tsai TL, Lin CA, Tseng TY (2014) Switching mechanism of double forming process phenomenon in ZrO_x/HfO_y bilayer resistive switching memory structure with large endurance. Appl Phys Lett 104:062901
23. Kim YJ, Yang BS, Oh S, Han SJ, Lee HW, Heo J, Jeong JK, Kim HJ (2013) Photobias instability of high performance solution processed amorphous zinc tin oxide transistors. ACS Appl Mater Interfaces 5:3255–61
24. Kim YH, Heo JS, Kim TH, Park SJ, Yoon MH, Kim JW, Oh MS, Yi GR, Noh YY, Park SK (2012) Flexible metal-oxide devices made room-temperature photochemical activation sol-gel films. Nature 489:128–132
25. Dupin JC, Gonbeau D, Vinatier P, Levasseur A (2000) Systematic XPS studies of metal oxides, hydroxides and peroxides. Phys Chem Chem Phys 2:1319–24
26. Lee AR, Bae YC, Baek GH, Im HS, Hong JP (2013) Multi-level resistive switching observations in asymmetric Pt/Ta_2O_{5-x}/TiO_xN_y/TiN/Ta_2O_{5-x}/Pt multilayer configurations. Appl Phys Lett 103:063505
27. Sun QQ, Gu JJ, Chen L, Zhou P, Wang PF, Ding SJ et al (2011) Controllable filament with electric field engineering for resistive switching uniformity. IEEE Electron Dev Lett 32:1167–9

28. Song YL, Liu Y, Wang YL, Wang M, Tian XP, Yang LM et al (2011) Low reset current in stacked AlO_x/WO_x resistive switching memory. IEEE Electron Dev Lett 32:1439–41
29. Waser R, Dittmann R, Staikov G, Szot K (2009) Redox-based resistive switching memories-nanoionic mechanisms, prospects, and challenges. Adv Mater 21:2632–63
30. Chen C, Gao S, Zeng F, Tang GS, Li SZ, Song C, Fu HD, Pan F (2013) Migration of interfacial oxygen ions modulated resistive switching in oxide-based memory devices. J Appl Phys 114:014502
31. Yang JJ, Miao F, Pickett MD, Ohlberg DAA, Stewart DR, Lau CN, Williams RS (2009) The mechanism of electroforming of metal oxide memristive switches. Nanotechnology 20:215201
32. Jeong DS, Schroeder H, Breuer U, Waser R (2008) Characteristic electroforming behaviour in $Pt/TiO_2/Pt$ resistive switching cells depending on atmosphere. J Appl Phys 104:123716
33. Goux L, Czarnecki P, Chen YY, Pantisano L, Wang XP, Degraeve R, Govoreanu B, Jurczak M, Wouters DJ, Altimime L (2010) Evidences of oxygen-mediated resistive-switching mechanism in $TiN/HfO_2/Pt$ cells. Appl Phys Lett 97:243509
34. Goux L, Chen YY, Pantisano L, Wang XP, Groeseneken G, Jurczak M, Wouters DJ (2010) On the gradual unipolar and bipolar resistive switching of $TiN\backslash HfO_2\backslash Pt$ memory systems. Electrochem Solid-State Lett 13:G54–G56
35. Yoshida C, Tsunoda K, Noshiro H, Sugiyama Y (2007) High speed resistive switching in $Pt/TiO_2/TiN$ film for nonvolatile memory application. Appl Phys Lett 91:223510
36. Kwak JS, Do YH, Bae YC, Im HS, Yoo JH, Sung MG, Hwang YT, Hong JP (2010) Role of interfacial TiO_xN_{1-x} layer and TiN electrode on bipolar resistive switching $TiN/TiO_2/TiN$ frameworks. Appl Phys Lett 96:223502